Mechanical characterization and modeling of the heavy tungsten alloy IT180

Mechanical characterization and modeling of the heavy tungsten alloy IT180

Martina Scapin

Highlights

Mechanical characterization of WHA alloy IT180 for nuclear applications

Compression and tension tests at different temperatures and strain-rates

Investigation of strain-rate and thermal softening sensitivities

Strength model calibration via multi-objective procedure

Comparison between different elasto-plastic strength models

Abstract

Pure tungsten or its alloys (WHA) find applications in several fields, especially due to the fact that these materials show a good combination of mechanical and thermal properties and they are commonly used in aerospace, automotive, metal working processes, military and nuclear technologies. Looking at the scientific literature, a lack in the mechanical characterization over wide ranges in temperature and strain-rates was found, especially for W–Ni–Cu alloys.

In this work, the mechanical characterization and the consequent material modeling of the tungsten alloy INERMET® IT180 were performed. The material is actually used in the collimation system of the Large Hadron Collider at CERN and several studies are currently under development in order to be able to numerically predict the material damage in case of energy beam impact, but to do this, a confident strength model has to be obtained. This is the basis of this work, in which a test campaign in compression and tension at different strain-rates and temperatures was carried out. The dynamic tests were performed using Hopkinson Bar setups, and the heating of the specimen was reached using an induction coil system. The experimental data were, finally, used to extract the coefficient of three different material models via an analytical approach.

Keywords

- Refractory metal;
- High temperature;
- High strain-rate;
- Hopkinson Bar;
- Johnson–Cook;
- Zerilli–Armstrong;
- Nuclear applications

1. Introduction

Pure tungsten or its alloys (WHA) find applications in several fields, especially due to the fact that these materials show a good combination of mechanical and thermal properties: high density, high mechanical strength also at high temperatures, high Young's modulus, moderate ductility, low thermal expansion, high thermal conductivity, good machinability and excellent resistance to corrosion. As a matter of fact, they are commonly used in aerospace, automotive, metal working processes, military and nuclear technologies. In more detail, these materials are often used for balancing, absorbing vibrations or source mass components [1]. They are also suitable for shielding, collimation [2] and [3] or target [4] and [5] components in medical, nuclear or industrial technologies: tungsten can provide the same effect as other materials, such as lead, but reducing the physical dimensions of the components. Tungsten alloys are finally appropriate in severe tooling applications, such as die casting, extrusion or in general, high temperature conditions. In military applications the WHAs are specialized as a kinetic energy penetrator since, for example, they represent a valid alternative to conventional depleted uranium penetrators, which are extremely environmentally unsafe materials [6], [7], [8], [9] and [10].

The high melting point of pure tungsten makes it impossible to apply the manufacturing techniques commonly used for other metals, such as melting and casting in a mold. In this case, a powder metallurgy technique is often used for the material production, in which the tungsten powders are mixed with the other low melting elements, such as copper, nickel, iron, cobalt, and chromium. The liquid phase sintering process implies that the mixed powders are compacted and then subjected to heat treatment below the W melting temperature. In this way, the lower melting elements melt forming the matrix that bonds the unmolten W particles together. In general, the result of the sintering process is a spheroidized microstructure, in which the rounded phase is pure tungsten surrounded by a metallic binder phase also containing dissolved tungsten (solid solution). The tungsten spheres show the typical BCC structure with a very high Young's modulus, while the binder phase has commonly a FCC structure and is responsible of the ductility of the resultant material. Therefore, the mechanical properties of the final alloy are mainly related to the complex interaction between the two phases as well as their own properties, depending also by the loading condition.

Generally, the tungsten heavy alloys are split into two wide categories: those with Ni–Fe and those with Ni–Cu as the binder phase. From a commercial point of view, one of the big suppliers, the Plansee company, names the W–Ni–Fe alloys (WNF) as DENSIMET®, while the W–Ni–Cu alloys (WNC) as INERMET®.

In this work the main goal was the mechanical characterization and the consequent material modeling of the tungsten alloy INERMET® IT180. The test campaign involved both compression and tension tests at different strain-rates and tension tests at different temperatures both in quasi-static and dynamic regimes. The obtained results were finally used to identify a suitable strength model for the mechanical behavior description. The motivation at the basis of this research was that INERMET® IT180 is currently used and under study as material in the collimation system of the Large Hadron Collider at CERN (Geneva, Switzerland). The collimators are devices which can directly interact with the high energy beam: the energy deposition on the bulk material could be potentially destructive for these components, generating the outgoing of shock-waves and deforming the material in very high strain-rate and temperature conditions [11]. The experimental phase in these extreme conditions is very expensive in terms of cost and

resources [12]. From this, the importance to be able to numerically simulate these events with a high level of confidence. To do this, it is necessary to define a proper strength model for the hit material, able to correctly reproduce the mechanical behavior over a wide range in strain-rate and temperature.

2. Bibliografic review

Looking at the scientific literature, the mechanical behavior of W–Ni–Fe alloys have been studied under several loading conditions for a long time, while fewer studies can be found for W–Ni–Cu alloys.

For WHA alloys, several works dealt with the mechanical characterization in compression [7], [8], [9], [10],[13], [14], [15] and [16],tension [4], [5], [17], [18], [19], [20], [21] and [22] or fatigue [4] and [5] at different temperatures [17], [18] and [22], strain-rates [7], [9], [15], [18] and [20] or both of them [8], [10], [13], [14], [16] and [19].

Some of the common results obtained from compression tests on WNF can be summarized as follows. The material is strain-rate and temperature sensitive [13] and [14], as expected for a BCC material [8],[9] and [15], and there is a mutual influence between theses effects (i.e., the thermal softening is not the same at different strain-rates or vice versa [9] and [13]). Up to medium-high strain-rates, the relation between stress and strain-rate seems to be logarithmic [13] and [14]: this highlights a deformation process based on thermal activation without a steep increase at very high strain-rates (change in the microstructural deformation mechanism). At very high strain-rates, different results were found: in some cases, as in [14] the behavior was logarithmic, in other cases, as in [9] a change in the deformation mechanism was found. The material is subjected to thermal softening at very high strain-rate, due to the heat conversion of plastic work [14]. The percentage of void and the roughness of the specimen surface play important roles in the determination of the material properties and this justifies the need to control and optimize both sintering and machining operations [5].

In the most part of the above mentioned works, also the fracture analysis was performed, analyzing the microstructure evolution and the crack propagation. As well explained in [14], in a sintered material, as those here analyzed, there are four possible fracture paths: the separation between tungsten grains at their interface, the separation at the interface between tungsten and binder phases, the cleavage inside a tungsten grain and, finally, the matrix failure. Depending on which of these failure modes becomes predominant, the strength and the ductility of the material are more or less pronounced. Different authors found that larger grain deformation occurs at high temperature or strain-rate [7] and [14]. Different failure modes were found from fractographic observation depending on the testing condition, but also on the quality of the materials coming from the sintering process. In some cases at low temperature and strain-rate the failure path was along the matrix and the tungsten–tungsten interfaces [9] without any cleavage in tungsten grains until high temperatures were reached [16]. At high strain-rates a more significant influence of microcracks formation and coalescence was found [13] and [15] and the brittle transgranular cleavage of tungsten grains becomes significant even if the matrix failure is still ductile [14] and [16]. In some cases, also an increase of voids coalesce was found at high temperature and low strain-rate [13]. In some studies, the experimental data were used to get the parameters identification for different strength material models[9], [10], [14], [16] and [18]. The most used strength models were: the Johnson–Cook (J–C)

model [23], the Zerilli–Armstrong (Z–A) model [24] or other models in which strain-rate and temperature are mutually related. The need of an ad-hoc model calibration comes from the fact that even if the amount of tungsten is high with respect the other elements, the model parameters obtained for pure tungsten do not fit the experimental data of the alloy. The strategies used for the coefficient determination could be the analytical data interpolation [9] and [14] or a numerical inverse approach.

A more limited number of works can be found for the mechanical characterization in tension. The data available show that no necking or limited necking occur at room temperature in quasi-static conditions [18]and that the most frequently fracture mode is the intergranular failure at tungsten–tungsten interfaces [5]. At high strain-rates the material softens increasing the strain and again the weakest point are the interfaces between tungsten grains where the failure starts in the direction perpendicular to the loading direction [20]. The results for WNC alloys show that this material is sensitive both in temperature and strain-rate and the deformation decreases increasing the strain-rate and reducing the temperature [19]. In [20] a crystal plasticity model within a failure model was applied to reproduce the experimental data. In [19] both Z–A and J–C model parameters were obtained by fitting the experimental data and the comparison demonstrated that the Z–A model was more suitable.

As it is easy to understand, the alloy chemistry influences the mechanical properties of tungsten alloys. From this it is possible to conclude that results obtained from WNF alloys could not be considered as valid for WNC ones. The problem is that in the authors' knowledge only few works are available for WNC alloys[4], [21] and [22]. In these works it was found that, the WNC alloys have much inferior tensile properties and hardness at room temperature: in more detail, both the material strength and the elongation at failure are lower. The cause is mainly related to the amount and the dimension of tungsten particles, which influences the fracture mode of the material. In [4] the microstructure and fractographic analyses of both the types of alloy demonstrated that the tungsten alloy with nickel and iron has smaller tungsten grains and a smaller amount of tungsten–tungsten interfaces. The dimension of the tungsten grains depends on the sintering temperature: the WNC alloys require higher temperature and this result is bigger grains [21]. This implies a lower amount of binder phase and an increase in the tungsten–tungsten interfacial area, which reduces the ductility, since it is the weak link in the microstructure.

3. Material under investigation & experimental setup

As previously mentioned in the Introduction, the final objective of this work is the numerical simulation of high energy beam impact against INERMET® IT180 components. Due to material thermo-mechanical properties within high Z number (70.83), it is actually used in the LHC as particles absorber to stop the last shower of particles before sensitive equipment. The material was supplied by Plansee and has the nominal composition of 95 wt.% W, 3.5 wt.% Ni and 1.5 wt.% Cu. As it is possible to see from the microstructure of Fig. 1, the W grains are quite big, with an average dimension of about 100 μm, which are surrounded by the binder phase, providing the necessary thermal and electrically continuity to the material.

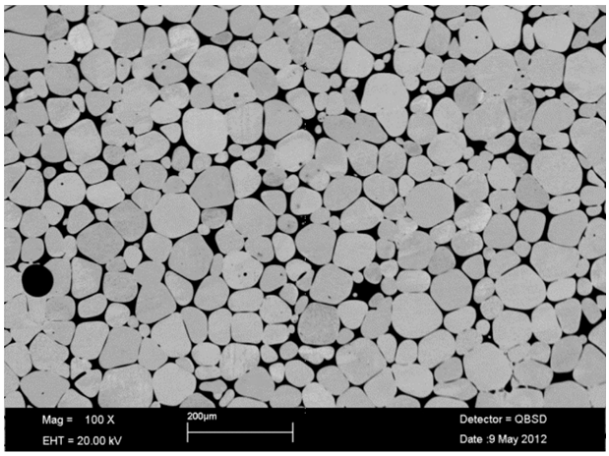

Fig. 1.
QBSD analysis at low magnification (100 ×) of IT180. The tungsten grains are clear while the binder phase appears black.

Since there is a big lack in the mechanical characterization of this alloy varying temperature and strain-rate over wide ranges, the author reports in this work the experimental results obtained from the test campaign, from which several strength material models were obtained.

The strain-rate and temperature are variables of fundamental importance for the definition of the mechanical behavior of materials. In some elastic–plastic models, the effects, coming from these two quantities, are considered to act independently. This approach allows greatly simplifying the experimental phase correlated to the parameter identification of the material model: the parameters for the strain-rate sensitivity could be extracted from tests at different strain-rates at a fixed temperature and the parameters for the temperature sensitivity could be extracted from tests at different temperatures at a fixed strain-rate.

In several applications, like in machining operation, metal forming, high energy impact or high energy deposition on metals, the materials are deformed at very high speed (which implies self heating due to adiabatic process) in high temperature condition. In this case, the stress vs. strain behavior comes as the result between the effects of hardening (due to strain and strain-rate) and thermal softening. In these cases, to consider the effect of strain-rate and temperature decoupled could not be acceptable. In this perspective, for the mechanical characterization of the IT180, a methodology for testing materials varying both strain-rate and temperature was applied, in accordance to the fact that in several studies it was found that, since the thermal softening and strain-rate sensitivity are mutually related, not always the thermal softening obtained from quasi-static tests could be applied to predict material response under dynamic loading conditions.

The mechanical characterization was performed both in tension and compression. A series of tests at room temperature at different strain-rates was performed (tension and compression) in order to obtain information about the strain and strain-rate sensitivity of the material. A series of tests at different temperatures in static loading condition (tension) was performed in order to obtain information about the thermal softening of the material. The atmosphere of the tests was air: the vacuum condition was not necessary, since the material did not experienced oxidation. The nominal temperatures of the tests were: 25 °C, 100 °C, 200 °C, 400 °C, 600 °C and 800 °C. A series of tests at different temperatures in high

dynamic loading condition (tension) was performed in order to obtain information about the thermal softening of the material at high strain-rate. The nominal temperatures of the tests were: 25 °C, 200 °C, 300 °C, 400 °C, 600 °C, 800 °C and 1000 °C. The test at 1000 °C was not performed in quasi-static condition since the test duration is too high and the testing equipment could not tolerate to remain to that temperature for long time; on the other hand the dynamic test duration is about 400 μs. The compression tests varying the temperature were not carried out since they are more difficult to be performed, due to the more significant influence of the friction at the contact interface between specimen and plates (or bars) of the testing equipment in the heating of the specimen.

For compression tests, a cylindrical specimen with a diameter of 4 mm and length of 4 mm was used while for tensile tests a dog-bone specimen (see Fig. 2) with gage diameter of 3 mm and gage length of 5 mm was adopted.

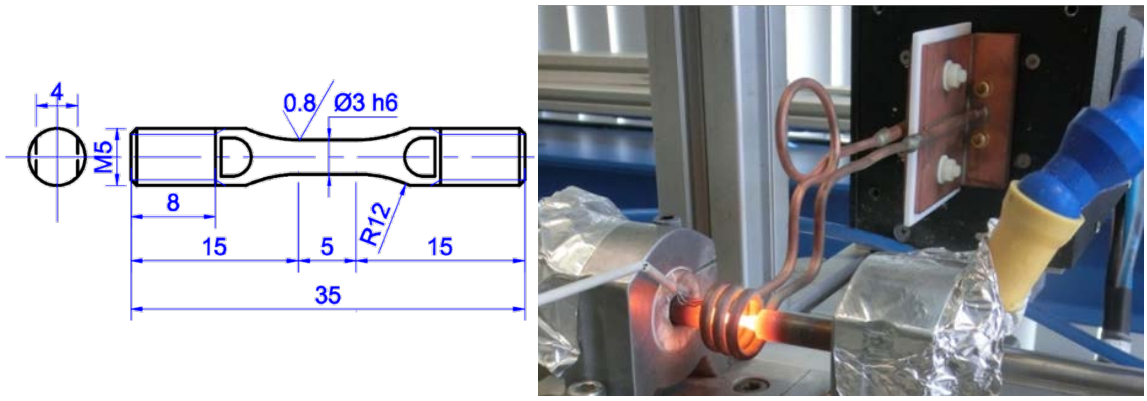

Fig. 2.
Sketch of the specimen used for tensile tests (d = 3 mm, L = 5 mm) and detail of the mounting on the direct tensile Hopkinson setup during a test at 600 °C: the thermocouples are used to control the temperature.

The low strain-rate tests were performed on a standard electro-mechanical testing machine Zwick Z-100 (maximum load 100 kN, maximum travel speed 5 mm/s). The medium strain-rate tests were performed on a standard servo-hydraulic testing machine Dartec HA100 (maximum load 100 kN; maximum speed 100 mm/s). The high strain-rate tests were performed using Split Hopkinson Bar setups. For both compression and tension tests direct setup was used: more details on them can be found in [25] and [26], respectively. The tests at different temperatures (see Fig. 2) were performed only for the tensile tests: both in quasi-static and dynamic regime, the specimen was heated using an induction coil system, controlled with a feedback on the temperature measurement obtained using thermocouples directly welded on the specimen surface [27].

4. Experimental results

For each testing condition at least three repetitions were performed in order to control the data scattering, but for the sake of clarity only the average curves are reported in the next diagrams. The estimation of the data scatter is performed in the next session and summarized in Table 1.

Table 1.

Data scatter evaluation in terms of NRMSE (%): tests at different temperatures (T) in quasi-static (10^{-3} s^{-1}) and dynamic (10^{3} s^{-1}) cases.

T (°C)								
SR (s^{-1})	25	100	200	300	400	600	800	1000
10^{-3}	0.93	0.15	0.39	NA	1.94	0.96	6.09	NA
10^{3}	1.98	NA	1.39	1.09	8.36	0.39	1.83	1.03

For each case, the load applied by the testing equipment and the stroke of the specimen were recorded. From the results in terms of force vs. displacements curves, considering the nominal (or measured, in case of compression) dimensions of the specimens, the engineering stress–strain curves of the material were obtained. Finally, starting from these data, analytically, under the assumption of volume conservation, true strain–true stress curves were obtained and then the elastic part of the deformation was subtracted. The results in terms of true stress vs. true plastic strain are reported in Fig. 3 in four diagrams: a) compression tests at room temperature varying the strain-rate, b) tension tests at room temperature varying the strain-rate, c) tension tests in quasi-static loading condition varying the temperature and d) tension tests in dynamic loading condition varying the temperature. For what concerns the tensile results, the last point of each curve corresponds to the maximum of the engineering stress: this justifies the analytical approach (neglecting the post-instability phase). The stress–strain analysis of the material response could also be done with a numerical inverse approach [28]: this technique allows treating the experimental results with a high level of accuracy, taking into account the effect of the geometry changes during the necking phase. For IT180, the necking phase is very limited (in many test conditions it is completely absent), hence a simplified analytical approach is sufficient and justified.

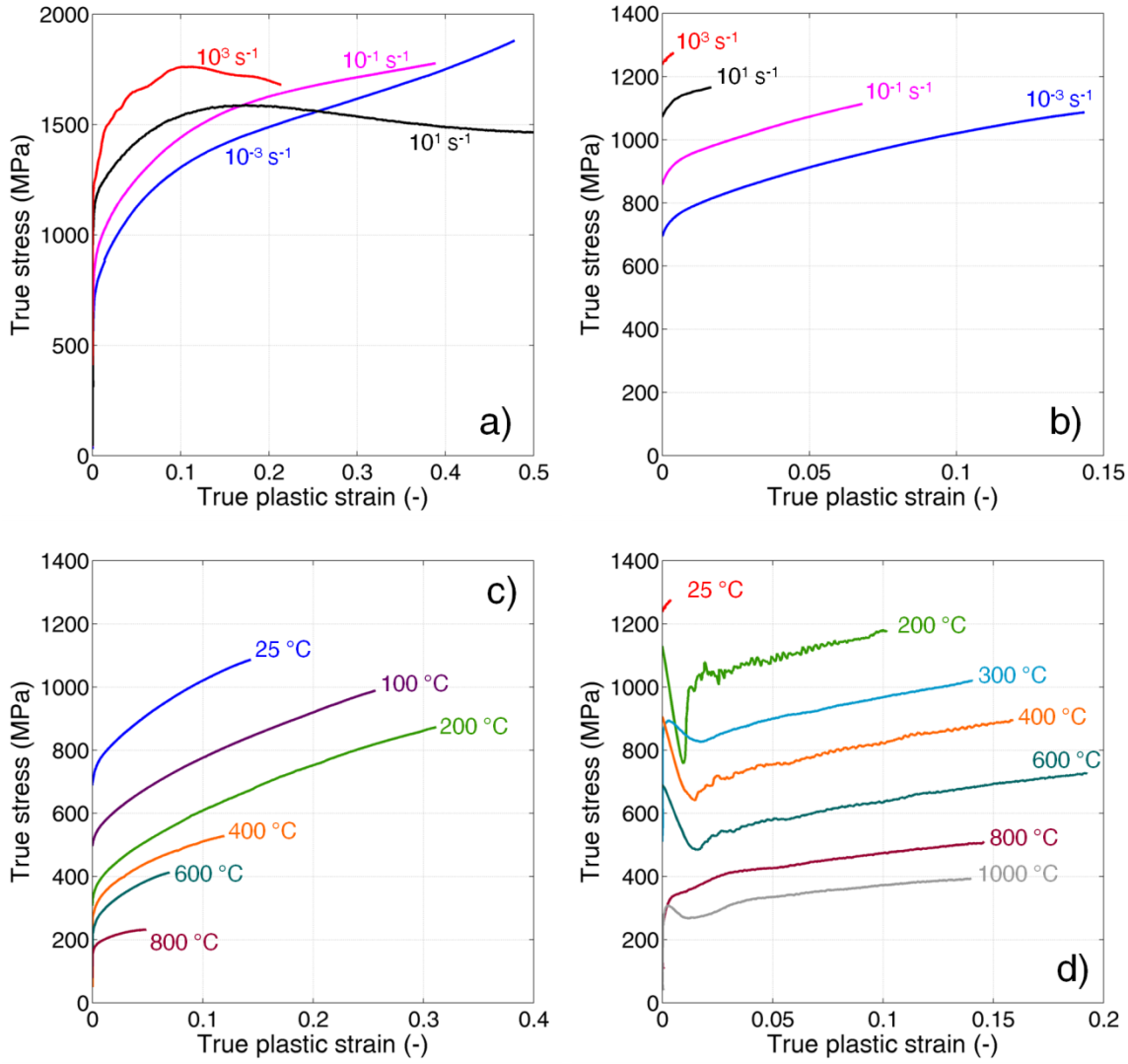

Fig. 3.

True stress vs. true strain curves obtained from the experimental test campaign (one curve is shown for each testing condition): a) compression tests at room temperature varying the strain-rate, b) tension tests at room temperature varying the strain-rate, c) tension tests in quasi-static loading condition varying the temperature and d) tension tests in dynamic loading condition varying the temperature.

Looking at the results, it is possible to notice that, as expected the material is temperature and strain-rate sensitive in both tension and compression. In particular, the sensitivity is that expected for BCC material: the yield stress is a function of temperature and strain-rate. The strain-rate increment implies the hardening of the material for low level of strain. Starting from medium-high strain-rate (above 10^1 s^{-1}), over a certain amount of deformation, the plastic work becomes relevant as well as the heat generated inside the specimen. In this condition, the thermal softening balances and overcomes the effect of the strain-rate hardening. This phenomenon can be clearly observed in compression, while in tension the material is too much brittle increasing the strain-rate at room temperature: maximum deformation at failure about 1%. On the contrary, at high strain-rate but increasing the temperature (at least at 200 °C), the material becomes more ductile, reaching deformation greater than 10%. Both in quasi-static and dynamic regimes, the strain

to failure (or equivalently the strain at which the instability starts) grows increasing the temperature, reaches a maximum and then decrease again for very high temperature.

For a more in-depth analysis of the thermal softening, the stress vs. temperature diagram at fixed values of (true) strain was obtained as reported in Fig. 4.a. The chosen values of strain were 1, 5, 10 and 15%: they are small values since a lot of curves do not reach a high level of deformation, but in any case they are sufficiently high to overcome the initial oscillation in dynamic tests. About the last point, as well explained in [29], the initial peaks in Hopkinson tests are due to inertia or misalignment and are not related to the material yield stress. For these reasons, they are neglected in the data analysis.

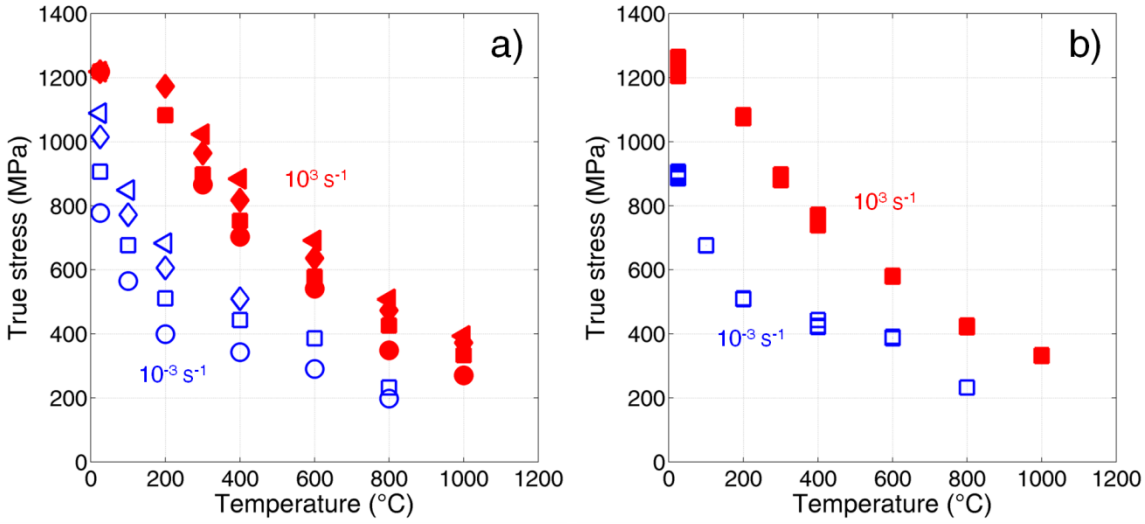

Fig. 4.

Temperature sensitivity in quasi-static (empty markers) and dynamic (full markers) loading conditions for tensile tests: a) at different levels of deformation: 1% (○), 5% (□), 10% (◇) and 15% (◁) for one test for each loading condition; b) evaluation of the data scatter at 5% of deformation for all the experimental tests.

Looking at the diagram of Fig. 4.a, it is possible to notice that the material behavior is such that, increasing the temperature, the material trend does not show a decrease of the hardening effect, differently from what can be found for other materials [26] and [30]. In order to analyze the data scatter of the material the same diagram is reported in Fig. 4.b at 5% of deformation for all the experimental tests. In this case, all the available data were used, hence it is possible to observe that the scatter is very low, except for high strain-rate test at room temperature, in which the brittleness makes the test less repeatable (the data refer to 1% of deformation).

Looking at the trend of the stress as a function of the temperature, it is possible to notice that the thermal softening at low and high strain-rate is slightly different. In more detail, in quasi-static case, saturation appears between 400 and 600 °C, while for higher temperatures (800 °C) there is a sharp drop in the material strength. On the contrary, in dynamic case, the material strength is continuously decreasing with temperature up to 1000 °C.

A similar analysis was also performed for the strain-rate hardening. Comparing the results obtained at different strain-rate in tension and compression (see Fig. 3), it is possible to appreciate the differences in

the material behavior coming from different loading states. In compression the material exhibits higher yield stress and strength and in addition a more significant hardening effect. In Fig. 5, the detailed analysis of the strain-rate sensitivity is reported. As made for tests at different temperatures, also in this case the stress values extracted at fixed strain (true) plastic strain (equal to 5%) are plotted as a function of strain-rate (semi-logarithmic plane). In the same diagram both compression and tension data are reported: as expected in both cases, the trend is linear up to nominal strain-rate of 10^3 s^{-1}. The most scattered results were obtained in compression probably due to friction effect. In any case, it is possible to notice that the strain-rate sensitivities in tension and compression are similar, obviously with different absolute values. Some differences could be explained by different deformation mechanisms.

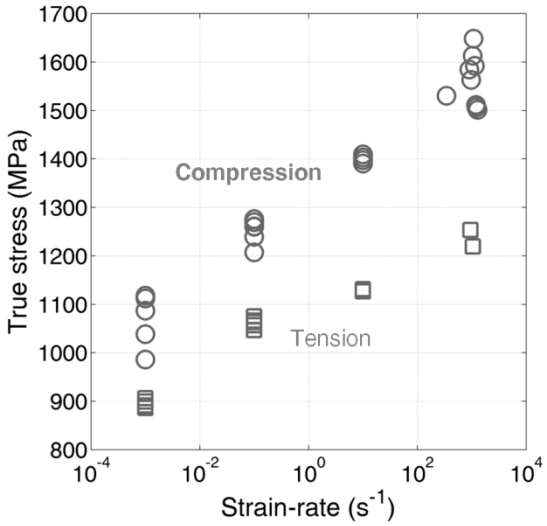

Fig. 5.

Strain-rate sensitivity in tension (□) and compression (○) and evaluation of the data scatter at 5% of deformation for all the experimental tests.

5. Material modeling

The experimental results showed the material is strongly dependent on strain, strain-rate and temperature. Moreover, strong coupling effects of temperature with strain as well as temperature with strain-rate were observed. From these reasons, it is important to find an appropriate material model for the mechanical behavior description. As it is well known, in the scientific literature, it is possible to find a great number of constitutive models for the viscoplastic flow description. Some of them are empirical models, while others are partially or completely physical-based. In [10], a comprehensive analysis was performed taking into account a considerably part of material models and their application to WHA alloys.

Between all the available models, J–C [23] and Z–A [24] are the most used. J–C is very simple and requires a few number of tests to be calibrated. It expresses the flow stress as:

$$\sigma_y = \left(A + B\varepsilon^n\right)\left(1 + C\ln\frac{\dot{\varepsilon}}{\dot{\varepsilon}_0}\right)\left(1 - \left(\frac{T - T_r}{T_m - T_r}\right)^m\right) \quad (1)$$

where ε is the equivalent plastic strain, $\dot{\varepsilon}$ is the plastic strain-rate adimensioned with respect to $\dot{\varepsilon}_0$ (equal to 1 s^{-1} in the original formulation), T is the actual absolute temperature expressed as a function of T_r and T_m, which are the reference and the melting temperatures, respectively. Finally, the model parameters are: A, B, n, C and m.

On the other hand, the Z–A model allows discriminating between FCC and BCC materials and coupling between temperature and strain-rate effects. For BCC materials, the formulation is:

$$\sigma_y = C_1 + C_2 e^{(-C_3 + C_4 \ln \dot{\varepsilon})T} + C_5 \varepsilon^n \tag{2}$$

in which the exponential part represents the thermally activated component of the flow stress, while the remaining part is the athermal component, with C_1 related to the dislocation mechanics and the grain dimension. In Eq. (2), ε represents the equivalent plastic strain, $\dot{\varepsilon}$ is the plastic strain-rate and T is the absolute temperature. The materials parameters are: C_1, C_2, C_3, C_4, C_5 and n.

For both these material models several modified formulations exist, with the aim to extend the range of application.

In this sense, for example in [30], the Z–A model was modified in order to find out a more suitable constitutive equation to model the flow stress in a wide range of temperature and strain-rate. Moreover, in this model, the coupling between strain and temperature was added to that between temperature and strain-rate. The model proposed in [30] has the following formulation:

$$\sigma_y = \left(C_1 + C_2 \varepsilon_{pl}^n\right) e^{-(C_3 + C_4 \varepsilon)T^* + \left(C_5 + C_6 T^*\right)\ln \dot{\varepsilon}^*} \tag{3}$$

in which T^* is the temperature increment with respect to the reference condition and $\dot{\varepsilon}^*$ is the ratio between actual and reference strain-rates. The first parenthesis represents the flow stress at reference temperature and strain-rate and, similar to the original formulation for BCC materials, the yield stress varies with temperature and strain-rate. The model parameters are: C_1, C_2, C_3, C_4, C_5, C_6 and n.

For three materials models (J–C, Z–A and Z–A modified) an analytical interpolation procedure was adopted for the parameters identification. In all the cases, a multi-objective procedure was used, in which at the same time the true stress vs. true plastic strain curves of all the experimental tests were used as targets. For each experimental curve, the normalized distance between the experimental data and the model prediction was calculated and then divided with respect to the number of points, as expressed in Eq. (4). Then the sum of all the normalized distances was minimized, varying all the model parameters. The response function was the sum of the normalized root mean square error (NMRSE) and is defined as follows:

$$f = \sum_{i=1}^{m} \sqrt{\sum_{k=1}^{n_i} \left(\frac{x_{i,k} - \hat{x}_{i,k}}{x_{i,k}} \right)^2 \frac{1}{n_i}} \tag{4}$$

where the index i identifies one of the m objectives, the index k identifies one of the n points of the i-th objective, x represents the experimental target and $\hat{x}$ represents the computed response.

In the calculation of the predicted response, the strain-rate of each test was assumed to be nominal, since in all the material models its influence is logarithmic, and the effect of the variation in less than one order of magnitude is limited. On the other hand, in case of dynamic tests (starting from 10^1 s^{-1}), the self-heating of the material was taken into account [10], so the temperature increment was expressed as a function of the cumulative amount of deformation energy converted into heat (dividing by density ρ and specific heat c_p):

$$\Delta T = \frac{\beta}{\rho c_p} \int_0^{\varepsilon} \sigma \, \mathrm{d}\varepsilon \tag{5}$$

in which the Taylor–Quinney coefficient β was assumed equal to 1.

The range in temperature in quasi-static condition was limited up to 400 °C: the experimental data obtained at 600 and 800 °C were not taken into account for the optimization process. This because, as explained before, the temperature influence in quasi-static condition has an S-shaped trend, which could not be reproduced by the considered models. This choice is justified also by considering the mechanical characterization at high strain-rates as the main goal.

The data scatter was evaluated using the definition of NRMSE, as reported in Eq. (4). For each testing condition, the percentage error was evaluated as the sum of the normalized distance of each repetition with respect to the mean curve. The results are summarized in Table 1.

5.1. Johnson–Cook

In the case of J–C model, the material constants were: $\dot{\varepsilon}_0$ = 1 s^{-1}, T_r = 298 K, T_m = 1673 K [31]. The optimized parameters were: A = 647 MPa, B = 1337 MPa, n = 0.5616, C = 0.0640 and m = 0.4937.

Fig. 6 compares experimental data and J–C model prediction for different loading conditions (also the quasi-static tests at high temperature are compared even if they were not used in the optimization). The error for each loading condition was evaluated in accordance to Eq. (4) and reported as histogram bars in Fig. 7.a: the height of the histogram is the average NRMSE evaluated for all the repetitions and the error bars are used to identify the standard deviation of the error. Except for the dynamic case at very high temperature, in which the error is greater than 20%, for the other cases the error is less than 10%. The predictability of the model is summarized in Fig. 7.b, in which the correlation between experimental and predicted flow stress is shown and evaluated equal to 0.9883.

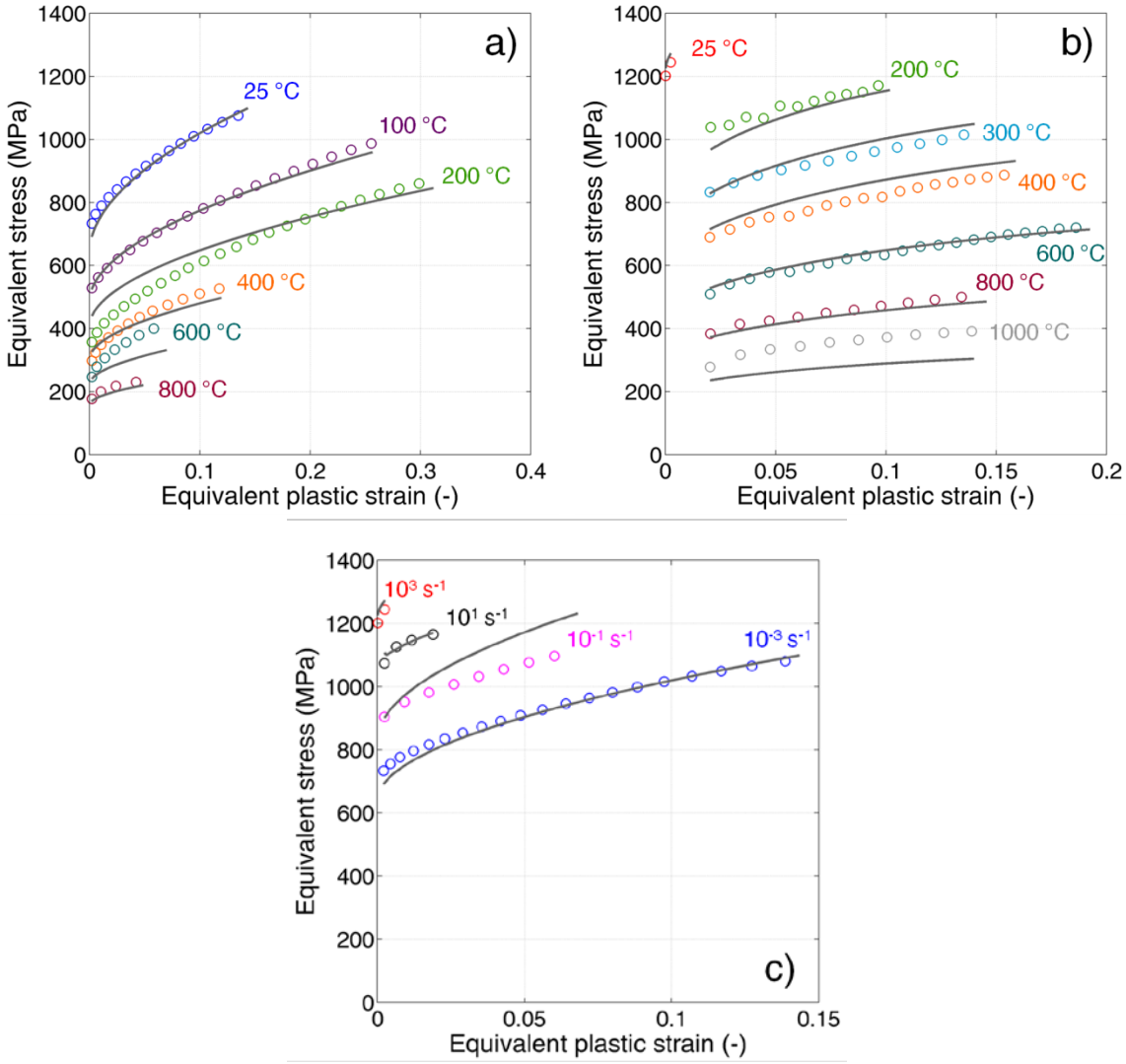

Fig. 6.

Comparison of experimental data and J–C model prediction for different loading conditions: a) quasi-static tests at different temperatures, b) dynamic tests at different temperatures, c) varying the strain-rate at room temperature.

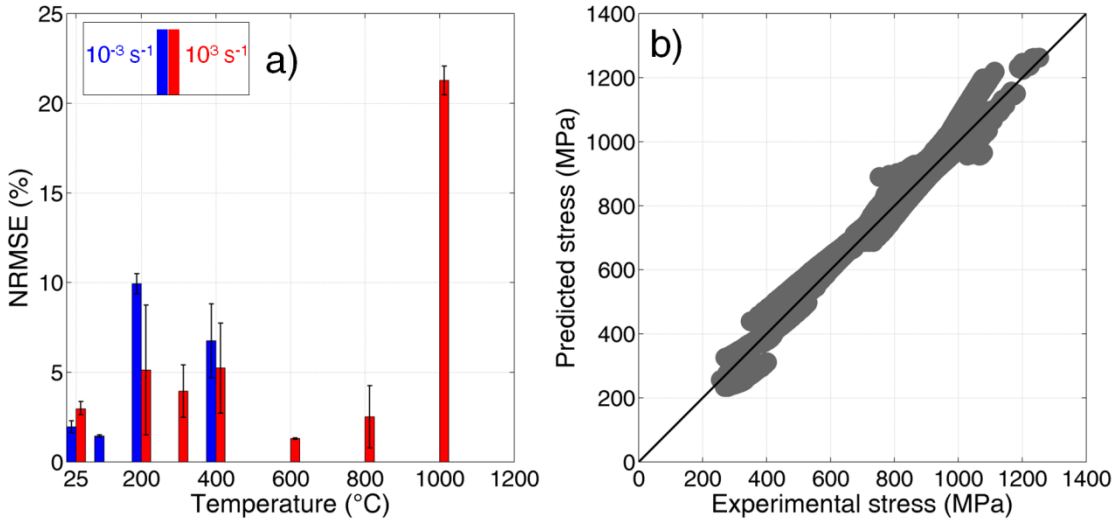

Fig. 7.

a) Evaluation of the Normalized Root Mean Square Error and its standard deviation as a function of temperature both for quasi-static and dynamic case (the histograms of dynamic test at 100 °C and quasi-static tests at 600, 800 and 1000 °C are missing); b) correlation between experimental and predicted stresses.

5.2. Zerilli–Armstrong

In case of Z–A model, the optimized parameters are: C_1 = 21 MPa, C_2 = 2572 MPa, C_3 = 3.416 × 10^{-3} K^{-1}, C_4 = 1.591 × 10^{-4} K^{-1}, C_5 = 915 MPa and n = 0.497.

Fig. 8 compares experimental data and Z–A model prediction for different loading conditions (also the quasi-static tests at high temperature are compared even if they were not used in the optimization).

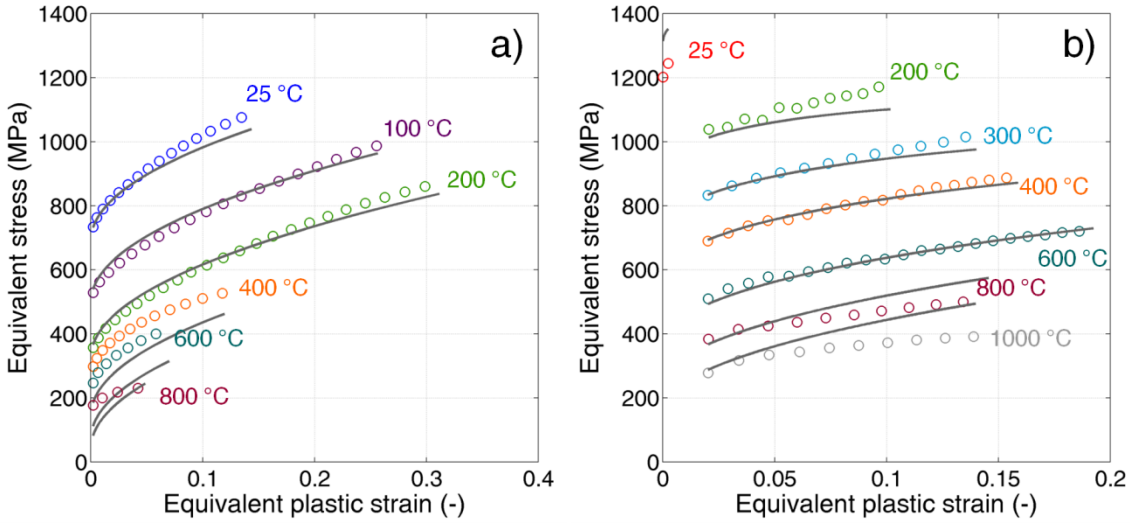

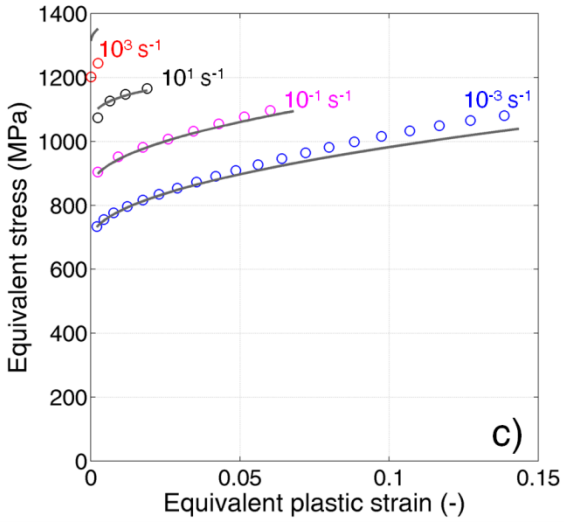

Fig. 8.

Comparison of experimental data and Z–A model prediction for different loading conditions: a) quasi-static tests at different temperatures, b) dynamic tests at different temperatures, c) varying the strain-rate at room temperature.

The error for each loading condition was evaluated in accordance to the Eq. (4) and reported as histogram bars in Fig. 9.a: the height of the histogram is the average NRMSE evaluated for all the repetitions and the error bars are used to identify the standard deviation of the error. Except for dynamic case at very high temperature and quasi-static case at 400 °C, in which the error is around than 20%, for the other cases the error is less than 10%. The predictability of the model is summarized in Fig. 9.b, in which the correlation between experimental and predicted flow stress is shown and evaluated equal to 0.9883.

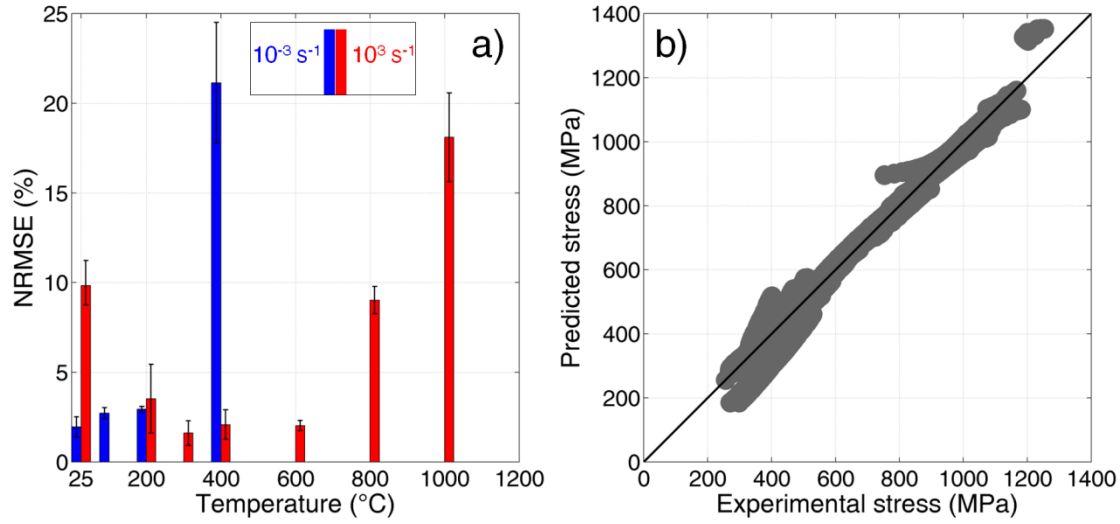

Fig. 9.

a) Evaluation of the Normalized Root Mean Square Error and its standard deviation as a function of temperature both for quasi-static and dynamic case (the histograms of dynamic test at 100 °C and quasi-static tests at 600, 800 and 1000 °C are missing); b) correlation between experimental and predicted stresses.

5.3. Modified Zerilli–Armstrong

In the case of the modified Z–A model, the material constants were: $\dot{\varepsilon}_0$ = 1 s^{-1} and T_r = 298 K. The optimized parameters are: C_1 = 708 MPa, C_2 = 726 MPa, n = 0.465, C_3 = 2.223 × 10^{-3} K^{-1}, C_4 = − 1.599 × 10^{-3} K^{-1}, C_5 = 3.636 × 10^{-2} and C_6 = 3.897 × 10^{-5} K^{-1}. Different from the results obtained in [30], here the parameter C_4 is negative: this is due to the hardening behavior at different temperatures, which implies an increment in the hardening rate with temperature.

Fig. 10 compares experimental data and modified Z–A model prediction for different loading conditions (also the quasi-static tests at high temperature are compared even if they were not used in the optimization). The error for each loading condition was evaluated in accordance to the Eq. (4) and reported as histogram bars in Fig. 11.a: the height of the histogram is the average NRMSE evaluated for all the repetitions and the error bars are used to identify the standard deviation of the error. Except for some quasi-static cases, in which the error is around than 10 ÷ 20%, for the other cases the error is around or less than 5%. The predictability of the model is summarized in Fig. 11.b, in which the correlation between experimental and predicted flow stress is shown and evaluated equal to 0.9912.

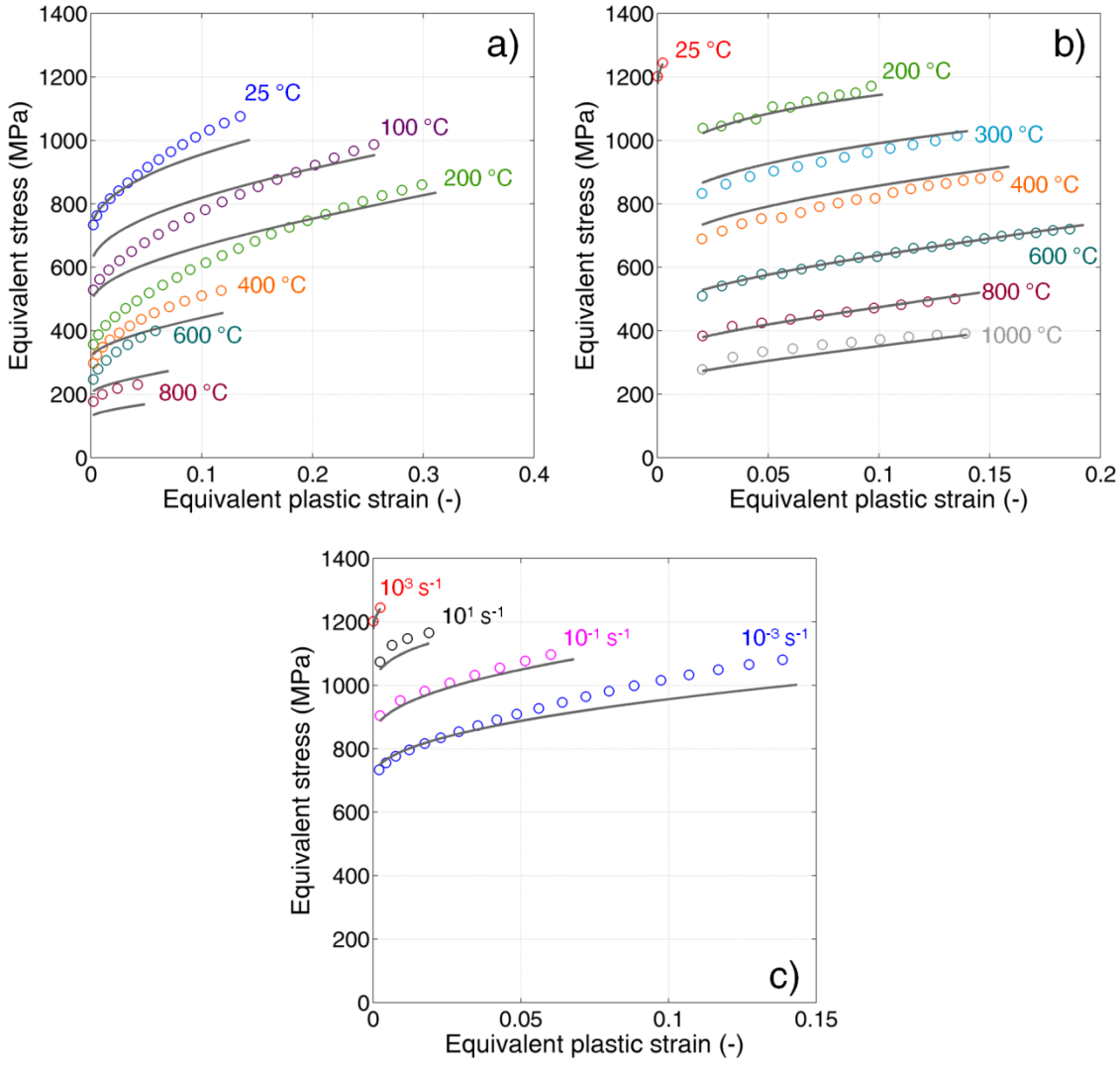

Fig. 10.

Comparison of experimental data and modified Z–A model prediction for different loading conditions: a) quasi-static tests at different temperatures, b) dynamic tests at different temperatures, c) varying the strain-rate at room temperature.

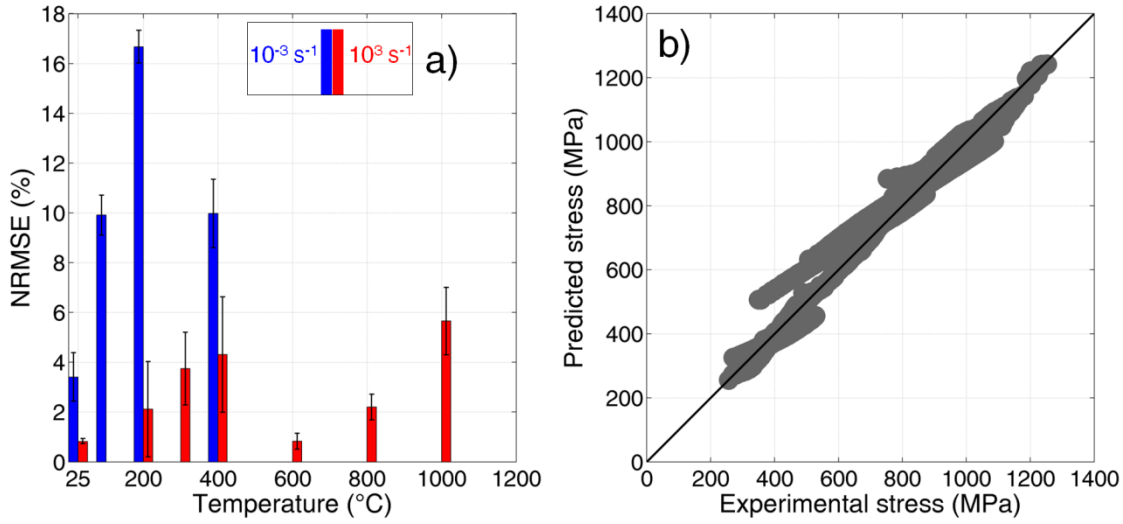

Fig. 11.

a) Evaluation of the Normalized Root Mean Square Error and its standard deviation as a function of temperature both for quasi-static and dynamic case (the histograms of dynamic test at 100 °C and quasi-static tests at 600, 800 and 1000 °C are missing); b) correlation between experimental and predicted stresses.

Looking at the results reported in Fig. 6, Fig. 7, Fig. 8, Fig. 9, Fig. 10 and Fig. 11, it is possible to conclude that all the investigated material models are able to partially reproduce the material response at different loading conditions. Looking at the Z–A models, the modified formulation implies a reduction of the error for all the loading conditions, so it represents the best solution. The modified Z–A model proposed is able to correctly reproduce the material behavior at high strain-rates over a wide range in temperature as well as the material response at different strain-rates at room temperature. The model is less accurate in the prediction of the behavior at different temperature in quasi-static regime, especially over 400 °C.

The modified Z–A model is finally applied also to compression results. Since the material behavior is different in tension and compression, two different models are needed: the model does not allow distinguishing the behavior as a function of the sign of the deformation. In any case, since experimental tests in compression varying the temperature were not performed, the coefficients directly related to the temperature, i.e., C_3, C_4 and C_6, were assumed equal to those found from the interpolation of the tensile experimental data. As previously performed for the dynamic compression tests, for tests at 10^1 and 10^3 s^{-1}, the adiabatic heating of the specimen was taken into account in the evaluation of the actual temperature as a function of the cumulative plastic energy of deformation (Eq. (5)). The optimized parameters are: C_1 = 21 MPa, C_2 = 1902 MPa, n = 0.173 and $C_5 = 2.528 \times 10^{-2}$. The parameter C_5 is similar to that

obtained from tensile tests (same order of magnitude): this means that the strain-rate effects are comparable in tension and compression even if some differences could be explained by different mechanisms at the basis of the deformation. On the other hand, the strain hardening behavior is, as expected, considerably different: in compression, the material strength is higher since the main contribution is given by the compression at the W grains.

Fig. 12.a compares experimental data and Z–A model prediction at different strain-rates. The error is evaluated in accordance to the Eq. (4) for each loading condition. The average value of the error is around 5% with the exception represented by tests at $10^{-3}\ s^{-1}$, which are the most scattered results. The predictability of the model is summarized in Fig. 12.b, in which the correlation between experimental and predicted flow stress is shown and evaluated equal to 0.9655.

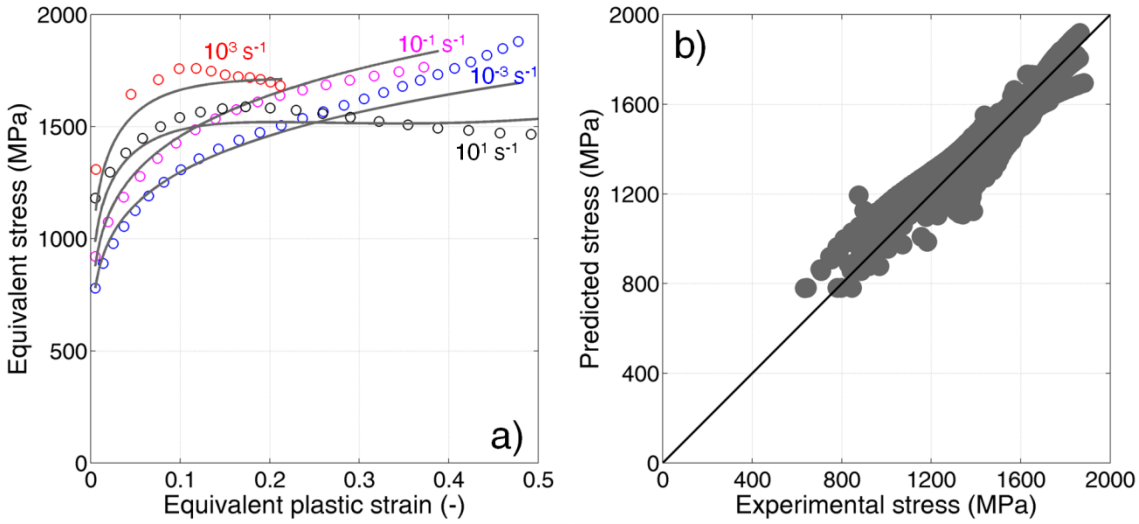

Fig. 12.

a) Comparison of experimental data and modified Z–A model prediction at different strain-rates in compression; b) correlation between experimental and predicted stresses.

6. Conclusions

The thermo-mechanical behavior of INERMET® IT180 was investigated under different loading conditions both in tension and compression. The strain-rates effects were investigated from 10^{-3} to $10^{3}\ s^{-1}$. For tensile tests also the temperature sensitivity was investigated over temperature ranging from 25 to 1000 °C in quasi-static and dynamic regime. The results showed that the material is both temperature and strain-rate sensitive. In more details, the effects were those expected for BCC pure metals. The flow stress expressed as a function of the temperature has a non-linear behavior with a different trend in quasi-static and dynamic case. The strain-rate produced a significant hardening of the materials over the entire investigated range, with a similar trend both in tension and compression. Obviously, due to the microstructure of this material, the mechanical response in tension and compression is completely different and governed by different interactions between grains and matrix, which is reflected in terms of absolute stress values, greater in compression.

The experimental data were used to obtain the coefficient for three material models, via an analytical approach, by fitting the true stress true plastic strain curves. For dynamic tests, the adiabatic self heating was taken into account. The chosen models were the purely empirical Johnson–Cook model and the partially physically-based Zerilli–Armstron model, in two different formulations: the original one and a modified version, in which a coupled effect between strain and temperature was added to that between strain-rate and temperature. For the description of the flow stress, the modified version of the Z–A model showed the lowest error values over the entire range of temperatures and strain-rates, as well as the maximum correlation coefficient between experimental and predicted flow stress. Finally, fixing the coefficient related to the temperature, a new interpolation was performed for the compression data and, also in this case, the obtained model was able to reproduce the experimental data with a good level of accuracy.

Acknowledgments

This work was performed within the WP 11 of the FP7 European Project EUCARD2. The financial support of the European Commission No: 312453 by means of the EUCARD2 Project is gratefully acknowledged. The author is grateful to the EN-MME Group of CERN, to Stefano Redaelli of BE-ABP of CERN and to Marija Cauchi from University of Malta for having provided the material and performed the microstructural analysis. The author is also grateful to Lorenzo Peroni and Claudio Fichera for their help and support in the experimental phase.

References

[1] Lamporesi G, et al. Source mass and positioning system for an accurate measurement of G. Rev Sci Instrum 2007; 78.

[2] Scapin M, Peroni L, Boccone V, Cerutti F. Effects of high-energy intense multi-bunches proton beam on materials. Comput Struct 2014; 141:74-83.

[3] Bertarelli A, et al. Behaviour of advanced materials impacted by high energy particle beams. J Phys Conf Ser 2013; 451.

[4] Lorenzo P, Miranda M, Iyengar S, Melin S, Noah E. Fatigue properties and characterization of tungsten heavy alloys IT180 & D176. Int J Refract Met Hard Mater 2013; 41:250-258.

[5] Pasalic M, Rustempasic F, Iyengar S, Melin S, Noah E. Fatigue testing and microstructural characterization of tungsten heavy alloy Densimet 185. Int J Refract Met Hard Mater 2013; 42:163-168.

[6] Leduc PR, Bao G. Thermal softening of a particle-modified tungsten-based composites under adiabatic compression. Int J Solid Struct 1997; 34(13):1563-1581.

[7] Ma Y, Liu JZW, Yue P, Huang B. Microstructure and dynamic mechanical properties of tungsten-based alloys in the form of extruded rods via microwave heating. Int J Refract Met Hard Mater 2014; 42:71-76.

[8] Kim DS, Nemat-Nasser S, Isaacs JB, Lischer D. Adiabatic shearband in WHA in high-strain-rate compression. Mech Mater 1998; 28:227-236.

[9] Yadav S, Ramesh KT. The mechanical properties of tungsten-based composites at very high strain rates. Mat Sci Eng A-Struct 1995; 203:140-153.
[10] Xu Z, Huang F. Thermomechanical behavior and constitutive modeling of tungsten-based composite over wide temperature and strain rate ranges. Int J Plasticity 2013; 40:163-184.
[11] Scapin M, Peroni L, Dallocchio A. Effects induced by LHC high energy beam in copper structures. J Nucl Mater 2012; 420(1-3):463-472.
[12] Bertarelli A, et al. An experiment to test advanced materials impacted by intense proton pulses at CERN HiRadMat facility. Nucl Instrum Meth B 2013; 308:88-99.
[13] Das J, Appa Rao G, Pabi SK, Sankaranarayana M, Sarma B. Deformation behaviour of a newer tungsten heavy alloy. Mat Sci Eng A-Struct 2011; 528:6235-6247.
[14] Lee W-S, Xiea G-L, Lin C-F. The strain rate and temperature dependence of the dynamic impact response of tungsten composite. Mat Sci Eng A-Struct 1998; 257:256-267.
[15] Zurek AK, GrayIII GT. Dynamic strength and strain rate effects on fracture behavior of tungsten and tungsten alloys. J Phys IV 1991; C3:631-637.
[16] Lee W-S, Lin C-F, Chang S-T. Plastic flow of tungsten-based composite under hot compression. J Mater Process Tech 2000; 100:123-130.
[17] Pink E, Kumar S, Grill R. Temperature-dependent deformation and fracture characteristics of a tungsten heavy metal. Int J Refract Met Hard Mater 1997; 15:301-309.
[18] Rohr I, Nahme H. Thoma K, Andersor Jr CE. Material characterisation and constitutive modelling of a tungsten-sintered alloy for a wide range of strain rates. Int J Impact Eng 2008; 35:811-819.
[19] Skoglund P. Material characterisation and constitutive modelling of a tungsten-sintered alloy for a wide range of strain rates. Scientific Report FOI-R-0723-SE 2002; ISSN 1650-1942.
[20] Weerasooriya T, Clayton J. Failure behavior of a tungsten heavy alloy at different strain rates under tensile loading. Proceedings of Int Conf on Tungsten, Refractory & Hardmetals VI 2006.
[21] Das J, Appa Rao G, Pabi SK. Microstructure and mechanical properties of tungsten heavy alloys. Mat Sci Eng A-Struct 2010; 527:7841-7847.
[22] McIntyre RD. Tungsten-Nickel-Copper ternaty alloys for high-temperature applications. NASA Technical Note D-3015 1965.
[23] Johnson GR, Cook WA. A constitutive model and data for metals subjected to large strains, high strain rates and high temperatures. Proceeding of 7th International Symposium on Ballistics 1983; 541-547.
[24] Armstrong RW, Zerilli FJ. Dislocation mechanics based analysis of material dynamic behaviour, J Phys IV 1998; 49:529-534.
[25] Peroni L, et al. Investigation of the mechanical behaviour of aisi 316l stainless steel syntactic foams at different strain-rates. Compos Part B-Eng 2014; 66:430-442.
[26] Scapin M, Peroni L, Fichera C. Mechanical Behavior of Glidcop Al-15 at High Temperature and Strain Rate. J Mater Eng Perform 2014; 23:1641-1650.
[27] Scapin M, Peroni L, Fichera C. Investigation of dynamic behaviour of copper at high temperature. Mater High Temp 2014; 31(2):131-140.
[28] Scapin M, Peroni L, Peroni M. Parameters identification in strain-rate and thermal sensitive visco-plastic material model for an alumina dispersion strengthened copper. Int J Imp Mater 2012;40-41:58-67.

[29] Borsutzky M, et al. Recommendations for Dynamic Tensile Testing of Sheet Steels. International iron and Steel Institute 2005.
[30] Samantaray D, Mandal S, Borah U, Bhaduri AK, Sivaprasad PV, A thermo-viscoplastic constitutive model to predict elevated-temperature flow behavior in a titanium-modified austenitic stainless-steel. Mat Sci Eng A-Struct 2009; 526:1-6.
[31] Mariani N. Development of Novel, Advanced Molybdenum-based Composites for High Energy Physics Applications. PhD Thesis, Politecnico di Milano 2014.